Agriculture, Ecosystems and Environment 254 (2018) 99–110

Contents lists available at ScienceDirect

Agriculture, Ecosystems and Environment

journal homepage: www.elsevier.com/locate/agee

Diverse sensitivity of winter crops over the growing season to climate and land surface temperature across the rainfed cropland-belt of eastern Australia

Jianxiu Shen[a,*], Alfredo Huete[b], Ngoc Nguyen Tran[b], Rakhesh Devadas[b], Xuanlong Ma[b], Derek Eamus[a], Qiang Yu[a,c,d]

[a] School of Life Sciences, University of Technology Sydney, NSW 2007, Australia
[b] Climate Change Cluster, University of Technology Sydney, NSW 2007, Australia
[c] State Key Laboratory of Soil Erosion and Dryland Farming on the Loess Plateau, Northwest A&F University, Yangling 712100, China
[d] College of Resources and Environment, University of Chinese Academy of Science, Beijing 100049, China

ARTICLE INFO

Keywords:
Climate variability
MODIS EVI
Crop growth stages
Land surface temperature
Rain-fed croplands
Eastern Australia

ABSTRACT

The rainfed cropland belt in Australia is of great importance to the world grain market but has the highest climate variability of all such regions globally. However, the spatial-temporal impacts of climate variability on crops during different crop growth stages across broadacre farming systems are largely unknown. This study aims to quantify the contributions of climate and Land Surface Temperature (LST) variations to the variability of the Enhanced Vegetation Index (EVI) by using remote sensing methods. The datasets were analyzed at an 8-day time-scale across the rainfed cropland of eastern Australia. First, we found that EVI values were more variable during the crop reproductive growth stages than at any other crop life stage within a calendar year, but nevertheless had the highest correlation with crop grain yield (t ha^{-1}). Second, climate factors and LST during the crop reproductive growth stages showed the largest variability and followed a typical east-west gradient of rainfall and a north-south temperature gradient across the study area during the crop growing season. Last, we identified two critical 8-day periods, beginning on day of the year (DoY) 257 and 289, as the key 'windows' of crop growth variation that arose from the variability in climate and LST. Our results show that the sum of the variability of the climate components within these two 8-day 'windows' explained > 88% of the variability in the EVI, with LST being the dominant factor. This study offers a fresh understanding of the spatial-temporal climate-crop relationships in rainfed cropland and can serve as an early warning system for agricultural adaptation in broadacre rainfed cropping practices in Australia and worldwide.

1. Introduction

As the world's fourth largest agriculture exporter, Australia, whose crop production accounts for over 13% of its export revenue (ABARES, 2017), has greatly influenced the world grain market in recent decades (Hamblin, 2009; Lawrence et al., 2013). Due to the interactions of three oceans, the Australian climate has the greatest variability among inhabited continents (Cleverly et al., 2016; Ma et al., 2016; Stokes and Howden, 2010; Xie et al., 2016). Rainfall, air temperature and solar radiation are direct growth-defining and limiting factors of broadacre crops (Yu et al., 2001), and their variability poses risks to Australian crop production in terms of reductions in harvest area (Cohn et al., 2016) and grain yield (Barlow et al., 2015; Zheng et al., 2012) as well as changes to the dates that define the crop growing season (Zheng et al., 2012). Recent studies have shown that Australian croplands, which are mostly characterized by a broadacre rainfed planting system, are vulnerable in grain production to current climate variability (Field et al., 2014; Tripathi et al., 2016). While the projected growth of the global human population necessitates an increased crop yield (Godfray et al., 2010; Hochman et al., 2017), growth in annual grain yield in Australia has stalled since 1990, which is majorly caused by the changing climate (Hochman et al., 2017). Thus, it is necessary to quantify the impacts of climate variability on crop growth and to take measures to enhance the development of agricultural early warning systems.

Climate-crop relationships have been intensively researched in recent decades. Based on a recent study, climate variation is responsible for approximately one-third (~32–39%) of global variation in crop yield (Ray et al., 2015). In Australia, climate variation in the state of

* Corresponding author.
E-mail address: Jianxiu.Shen@student.uts.edu.au (J. Shen).

https://doi.org/10.1016/j.agee.2017.11.023
Received 20 May 2017; Received in revised form 23 November 2017; Accepted 24 November 2017
0167-8809/

New South Wales (NSW) accounted for 31–47% of inter-annual wheat yield from 1922 to 2000 (Wang et al., 2015a). The results of crop simulations (Asseng et al., 2011) have indicated that variations of 2 °C of the average temperature during the crop growing season can cause up to a 50% reduction in grain production in Australian croplands. Under projected future climate scenarios, wheat yield will decrease by approximately 25% because of the predicted increase of temperature in southeastern Australia in future decades (Anwar et al., 2007). In most previous studies, the approaches of climate-crop relationship can be divided into two major types: observational and statistical models, and crop simulation techniques. The observational and statistical models have been based on data collected from administrative boundaries, which do not reflect the crop-growing process and do not explicitly reflect the spatial relationships identified. Although crop simulation techniques can precisely reconstruct the growth cycles of crops using parameter pre-setting, it is labor intensive to spatially up-scale the simulations from the field plot to ecosystem or regional scales (Rosenzweig et al., 2013). This is due to the fact that crop simulation needs considerable efforts in data collection and parameter calibration to overcome its limitations in spatial heterogeneity.

These limitations in spatial up-scaling can be overcome by introducing remote sensing detection methods (Reed et al., 1994; Sakamoto et al., 2005) or by combining crop models with satellite observations (Ma et al., 2008; Moulin et al., 1998). Satellite radiometric observations offer the advantage of multiple spatial, temporal and spectral resolutions and the data are from real-time observations (Eamus et al., 2016), which can characterize the full profile of the vegetation growth cycle. Remote sensing methods that have been utilized for crop-climate relationships often focus on estimating the cropland area (Biradar et al., 2009; Potgieter et al., 2011; Wardlow and Egbert, 2008) and detecting vegetation green-up and green-fade dates (Guo et al., 2016; Sakamoto et al., 2013). However, every stage of the crop growth cycle can impact the final crop yield. Currently, there is little knowledge about the different responses of crop performance to regional climate variability at each growth stage.

Understanding the impacts of climate on crop growth over its life span can help farmers and agricultural departments make timely decisions in response to climate variability and reduce potential losses in yield (Rabbinge, 2007) in broadacre rainfed cropping systems in Australia and worldwide. Thus, there is a need to illustrate the relationships between variations in several climate factors and crop growth throughout all crop growth stages and to identify the most sensitive 'windows', that is, the time segments of crop-growth that are most sensitive to climate variability.

Vegetation Indexes (VIs) are widely used remote indicators that characterize the status of land surface vegetation as well as the biophysical properties on global and regional scales (Karnieli et al., 2010; Wan et al., 2004). The VIs measure the 'greenness' of the canopy and monitor vegetation growth and health at various spatial scales (Huete et al., 2002; Ma et al., 2015). The Enhanced Vegetation Index (EVI) used in this study is an optimized VI that can effectively reduce soil background and atmospheric effects (Huete et al., 2002; Huete, 2012; Suepa, 2013).

Rainfall, air temperature and radiation influence crop canopy greenness by directly and indirectly controlling crop transpiration and photosynthesis (Calzadilla et al., 2013; Eamus et al., 2016) within the soil-plant-atmosphere continuum. Both the vegetative growth and reproductive growth stages of crops are dependent on and affected by these factors. The direct effects of variations in these factors on crop growth can be dominant during different growth stages. However, the proportion of the indirect effects of the complex interactions among these factors (Yu et al., 2014) on crops cannot be explained without a comprehensive indicator of the crop water and heat status. The radiative canopy temperature, (the Land Surface Temperature (LST)), is designed to measure the physical processes of the ground surface energy and water balance (Li et al., 2013) and reflects the water and heat status of vegetation and soil. In most cases, a high LST indicates deficient soil moisture and a high canopy heat stress (Karnieli et al., 2010). Thus, we introduced LST as a potentially crop-limiting climate component to describe the indirect impacts of rainfall, air temperature and solar radiation on crop growth.

This study investigated regional inter-annual variations in climate-crop growth relationships by incorporating MODIS land cover maps, time-series Enhanced Vegetation Index (EVI) and Land Surface Temperature (LST) products, ground meteorological station data and *in-situ* trial data across the rainfed cropland belt in NSW during the period from 2001 to 2013. An 8-day time-scale is applied as this is the attainable time step for the satellite that provides the data to produce MODIS EVI and LST. The objectives of this study are to: (1) identify the seasonality, trends and variability for EVI and each climate component during the crop growing season; (2) evaluate the individual and collective impacts of climate and LST variability on crops at the pixel and regional levels; and (3) investigate the relative contribution of the variability of each climate component to variation in crop growth during each 8-day time segment.

2. Materials and methods

2.1. Study area

The land cover map used in this study was obtained from the Dynamic Land Cover Dataset (DLCD) for Australia (http://www.ga.gov.au/) developed by Geoscience Australia. This dataset is based on an analysis of a 16-day MODIS EVI composite at a 250-m resolution during 2000–2008 (Lymburner et al., 2010). The dataset distinguishes rainfed cropland from irrigated cropland in Australia and shows a high degree of consistency (93%) with extensive independent field-based investigations.

Australian rainfed croplands (Fig. 1a) extend over 24.6 million hectares in a crescent around eastern, southern and western Australia and produce approximately 22.9 million tons of grain per year (www.abares.gov.au, 2013). Wheat is the major agriculture commodity across the rainfed cropland belt in Australia (Hochman et al., 2017). The NSW cropland belt (Fig. 1b) stretches across the drier western face of the Australian Great Dividing Range. It accounts for 27.5% of the wheat planted area in Australia and 27% of the total wheat production of the nation (www.abares.gov.au, 2013–14), which makes NSW the second-highest wheat producing state in Australia. The NSW wheat belt (Fig. 1c) has an average elevation of 287.8 m and a gradient of 50 to 750 m from west to east. The annual wheat production during the period from 2003 to 2014 varied between 2.48 and 10.49 million tons, and the yield varied by approximately 5-fold (0.62–2.75 t ha^{-1}) (www.abares.gov.au, 2013–14). Historically, wheat production in NSW has shown vulnerability to climate variability due to high exposure to water and heat stresses (Wang et al., 2015b). The mean annual air temperature and rainfall across the entire cropland belt of NSW vary between 12 and 20 °C and 250–800 mm, respectively, highlighting the significant spatial variation in climate conditions and revealing the complexity of modelling crop yields across broad spatial extents.

2.2. Data processing

2.2.1. Meteorological data and study sites

The meteorological station-based observational data from the Scientific Information for Land Owners (SILO) patched point dataset (http://www.bom.gov.au/silo/) for NSW were collected, and we extracted 161 study sites that were identified as being located in rainfed cropland pixels; both their ground meteorological data and spatially observed data were available. These sites are evenly distributed across our study area (Fig. 1b). As climate-driving parameters, daily rainfall (Rain), maximum air temperature (T_{max}), minimum air temperature (T_{min}), and solar radiation (Radn) from 2000 to 2014 were extracted for

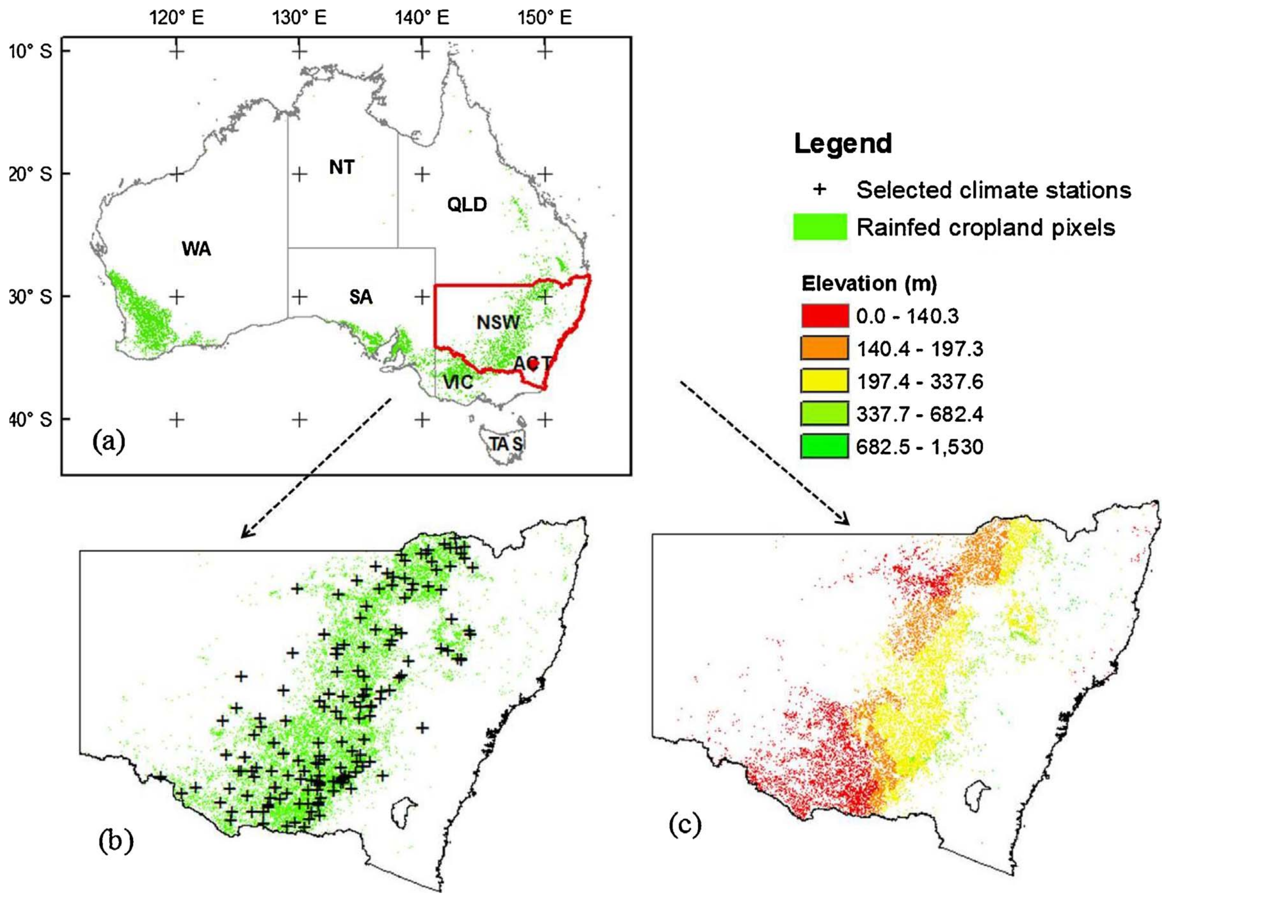

Fig. 1. Spatial distribution of the NSW rainfed cropland belt and locations of selected testing pixels. The green areas are the gridded rainfed cropland belts across Australia (a) and NSW (b); (c) elevation map of the NSW rainfed cropland belt. (For interpretation of the references to color in this figure legend, the reader is referred to the web version of this article.)

each site. We then up-scaled them to an 8-day time series to remove outliers and noise as well as to match the temporal resolution with remote sensing datasets. We averaged the 8-day Rain, T_{max}, T_{min} and Radn from the 161 sites to represent the generalized climate patterns of the time series across the NSW wheat belt.

2.2.2. Remote sensing and in-situ datasets

Approximately 14 years (February 2000–December 2014) of 16-day Terra-MODIS EVI data (MOD13A1) at a spatial resolution of 500 m and of 8-day Terra-MODIS LST (MOD11A2_day) with a 1000-m resolution were obtained online from the NASA Land Processes Distributed Active Archive Center (LP DAAC). The original data were then filtered based on the Quality Control layers along with the MOD13A1 and MOD11A2_day data. To unify the spatial and temporal resolutions of these 2 remote sensing datasets, the EVI values were interpolated and filled to achieve an 8-day series using the spline method, and the LST were resampled to a 500-m spatial resolution (Broich et al., 2015). Time-series profiles of the 500 m EVI and LST for the selected 161 cropland pixels were then extracted.

The integrated EVI (iEVI) has been widely used to represent vegetation productivity (Ma et al., 2015; Ponce Campos et al., 2013), which refers to the area under the EVI curve in a growing season. Here, we used iEVI to illustrate the spatial variation of accumulated aboveground biomass during the growing season. The iEVI and average climate conditions during the crop growing season at each selected pixel were calculated and interpolated using the inverse distance weighting (IDW) interpolation method over the study area.

The *in-situ* wheat trial (2005–2013) datasets were obtained from the Grains Research and Development Corporation (GRDC) National Variety Trials (NVT), Australia (http://www.nvtonline.com.au/). The sowing date, harvest date, and actual yield of separate groups of wheat trials for each year from 2005 to 2013 were recorded. There were 117 trial sites collected in total, and they were evenly distributed across the NSW croplands.

2.2.3. Phenology metrics detection

We discriminated the green-up (start of season, SOS), green-fade (end of season, EOS) and peak dates (peak of season, POS) of the growing season from the 8-day MODIS EVI time series profile using the following rules: (i) daily EVIs were reconstructed by using the Polyfit-Maximum method (Cong et al., 2013; Piao et al., 2006) with a degree of 9; (ii) the inflection point of the maximum of the second derivative during winter (from May to August) was identified as the SOS (Gong et al., 2015), while another inflection point during summer (from November to the end of year) was identified as the EOS; and (iii) the POS was identified as the date with the maximum EVI value during the growing season (Ma et al., 2013).

As for cropland, we assumed that the start of season (SOS), end of season (EOS) and peak of season (POS) dates were the leaf emergence, crop harvest and crop heading dates observed from remote sensing, respectively (Sakamoto et al., 2005). The length of the growing season (LOS) in this paper was defined as the difference between the SOS and EOS. The growing season (GS) was divided into the two stages of vegetation growth (VG) and reproductive growth (RG) by the POS date.

2.3. Methodology

2.3.1. Variability indicator

Mathematically, in the time series profile of EVI, technological improvements in farming practices (inter-annual trend), phenology

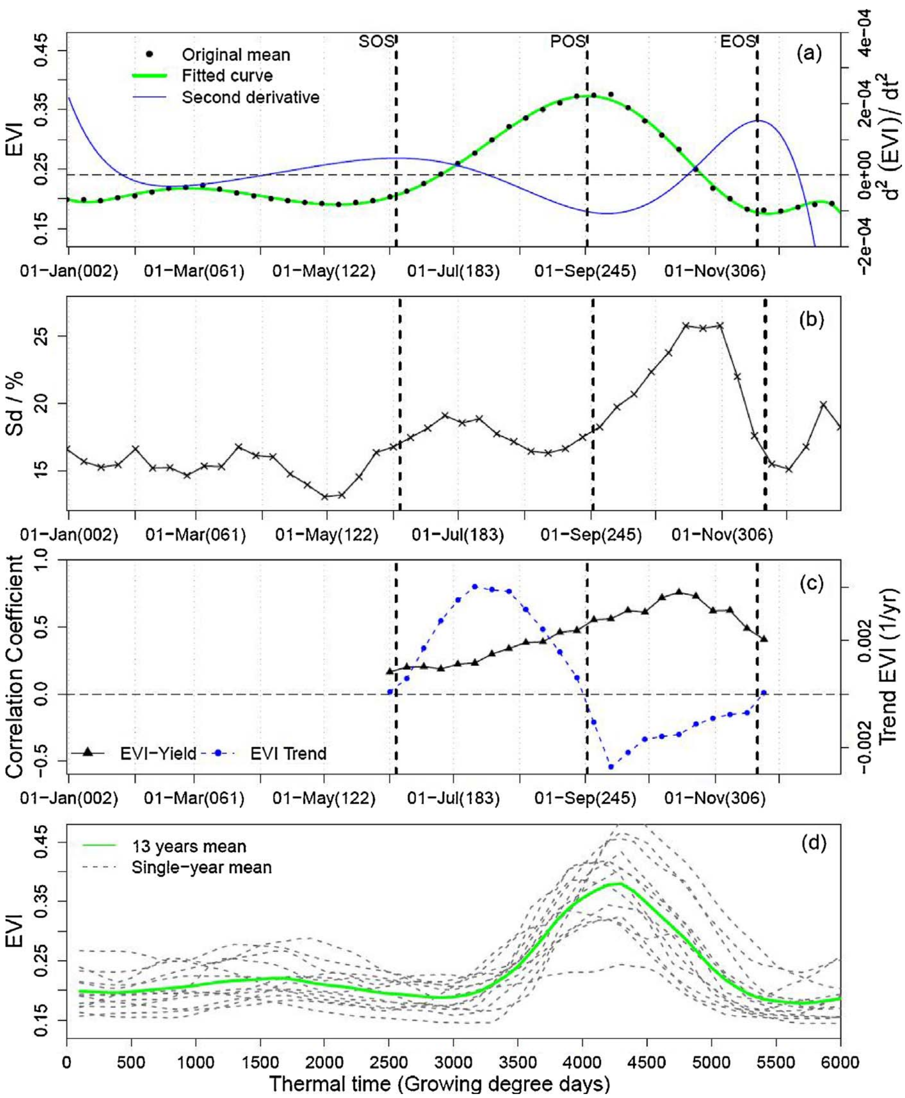

Fig. 2. Variation and trend of the average seasonal EVI profile in the NSW rainfed cropland belt from 2001 to 2013 and correlations of the 8-day EVIs with observed annual grain yield. (a) Black dots: average EVI values for all of the testing points from 2001 to 2013; green solid line: fitted EVI curve; blue solid line: second derivative; POS: peak of season (heading date); SOS: start of season (leaf emergence date); EOS: end of season (harvest date). (b) One standard deviation (Sd in %) of the 13-year period. (c) Blue dashed line with circle solid dots: EVI trends at each 8-day time point from 2001 to 2013. Black solid line with triangular solid dots: correlations between the 8-day EVIs and annual grain yield at 117 trial sites. X-axis of (a)–(c): Date (Day of the Year). (d) green solid line: 13 years mean EVI in the time reference of thermal time (growing degree days, °C). grey dashed lines: single-year means of EVI from 2001 to 2013. (For interpretation of the references to color in this figure legend, the reader is referred to the web version of this article.)

(seasonality, the time of turning points in crop growth and development), the vegetation variation caused by climate variability (inter-annual variation), and the system observational errors are subject to trend, seasonal, anomaly and noise components (Shumway and Stoffer, 2010), respectively. Here, the noise component can be reduced by unifying the temporal and spatial scale of EVI and LST. We assumed the technology in farming practices was at an average level from 2001 to 2013 and adopted a standardized anomaly (Sa-s) to represent the inter-annual variability of EVI, and similarly to each of the other variable.

$$x'_{d,y} = (x_{d,y} - \bar{x}_d)/\bar{x}_d \tag{1}$$

$x_{d,y}$ is a single element of a time-series variable X; x' is the anomaly value of each variable at the dth 8-day time point in the yth year; and $\bar{x}$ is the mean value at the dth 8-day time point throughout the period from 2001 to 2013. The time series sequence of Sa-s excluded the seasonality of the original data sequence without collinearity with the other variables. The 8-day Sa-s values of Rain, T_{max}, T_{min}, Radn, LST and EVI for the 161 selected points during 2001–2013 were calculated.

2.3.2. Thermal time reference

Converting the time reference from normal calendar time to thermal time allows to make an average consideration of crops in similar phenological stages among different years, and to remove the effects of spatial heterogeneity (Duveiller et al., 2013a,b). The thermal time theory is based on the time taken of plant growth and development, depending on temperature (Atwell, 1999). Therefore, thermal time (tt) over a particular time period from t_1 to t_2 can be expressed as cumulated heat units (in growing degree days) (Duveiller et al., 2013a,b; Franch et al., 2015; Skakun et al., 2017):

$$tt = \sum_{i=t_1}^{t_2} \left[\frac{(T_{\max,i} + T_{\min,i})}{2} - T_{base} \right] \tag{2}$$

In this case, the minimum (T_{min}) and maximum (T_{max}) air temperature are based on a daily time step. The base (T_{base}) temperature for winter wheat was set to 0 °C, and thestarting date t_1 was arbitrarily fixed to 1st January of each year from year 2001 to 2013. If the average daily air temperature of T_{max} and T_{min} is below T_{base}, it would be replaced by T_{base}, and no growing degree days are accumulated. Thermal time of EVI profiles were then calculated for each year but having irregularly sampled time series. To make them comparable, a regular sampling steps of 100 growing degree days were thereafter linearly interpolated (Duveiller et al., 2013a).

2.3.3. Relative importance approach

To elucidate the unique correlation between a single climate component Sa-s and EVI Sa-s without interference from other variables, we applied the partial correlation method (Chevan and Sutherland, 1991) by controlling the variance of the other 4 climate components. The package 'relaimpo' in R (Grömping, 2006) was applied to calculate the

Table 1
Seasonal climate and LST conditions each year across the rainfed cropland in NSW. (For interpretation of the references to color in this table, the reader is referred to the web version of this article.)

	Pre-GS					VG					RG				
	Rai mm	T_{max} °C	T_{min} °C	Radn MJ	LST °C	Rai mm	T_{max} °C	T_{min} °C	Radn MJ	LST °C	Rai mm	T_{max} °C	T_{min} °C	Radn MJ	LST °C
2001	1.18	28.9	14.0	20.3	32.5	1.16	16.8	3.9	11.8	15.6	1.29	23.6	9.24	20.8	30.3
2002	1.07	28.6	13.7	20.5	32.5	0.53	17.9	3.5	12.8	18.7	0.51	26.8	10.2	23.3	36.8
2003	1.07	28.6	14.8	20.3	33.6	1.46	16.4	4.5	11.8	15.7	1.07	23.4	8.59	21.9	30.1
2004	0.94	29.5	13.9	21.0	34.0	1.26	16.1	4.0	11.6	15.4	1.60	23.9	9.19	21.6	31.1
2005	0.62	29.2	13.6	21.1	34.0	1.87	16.8	4.9	11.8	15.8	2.16	24.2	10.4	20.7	27.9
2006	0.67	29.6	14.1	21.0	32.9	0.93	17.1	3.1	12.6	17.0	0.59	26.7	9.88	23.5	36.3
2007	1.15	29.6	15.5	20.3	34.4	0.95	16.5	4.0	12.1	16.4	0.83	26.1	10.3	22.1	34.5
2008	1.06	27.8	13.3	20.7	31.9	1.07	16.7	4.4	11.5	16.2	1.61	25.0	10.2	21.4	31.1
2009	1.03	28.9	14.5	20.6	33.3	1.05	17.2	5.2	11.4	16.2	0.80	26.7	10.9	21.4	33.9
2010	1.95	28.4	14.7	19.4	30.9	1.97	15.6	4.8	10.7	14.1	2.42	22.6	9.84	19.8	25.2
2011	1.69	27.8	13.8	19.3	28.8	0.83	17.5	4.0	11.8	16.6	1.73	24.8	9.96	20.5	29.6
2012	2.10	27.0	12.8	19.5	28.7	1.10	16.6	3.1	12.1	15.7	0.62	25.2	8.39	22.4	31.9
2013	1.08	29.1	14.1	20.7	33.1	1.28	17.8	5.1	11.6	16.9	0.76	26.2	9.19	23.1	33.1
Mea	1.20	28.7	14.0	20.4	32.3	1.19	16.8	4.2	11.8	16.2	1.23	25.0	9.73	21.7	31.7
Sd	0.43	0.77	0.66	0.58	1.79	0.38	0.63	0.6	0.51	1.03	0.60	1.35	0.73	1.08	3.13

*Pre-GS was calculated as the period from the first day of the year to Start of Season (SOS) at day 156. Sd is one standard deviation in each crop growth stage from 2001 to 2013. Red, yellow and green correspond to the order of the variable values from high to low among the pre-growing season (Pre-GS), vegetative growth phase (VG) and reproductive growth phase (RG).

ranks of the climate components for each 8-day time segment in terms of their unique contribution to EVI variation. Their unique contributions were then rescaled to sum to R^2, the total proportion of EVI variance explained by climate variability, as the relative contribution of the climate components. The individual and accumulated relative contributions of the selected climate variable Sa-s to the EVI Sa-s in the growing season both across study area and at each testing pixel were then calculated.

In this paper, data processing and statistical analysis were performed in the R computation environment, and related packages were obtained from The Comprehensive R Archive Network (http://cran.r-prject.org).

3. Results

3.1. Crop growth seasonality and variability across the NSW wheat belt from 2001 to 2013

3.1.1. Crop growth seasonality and variability

The average annual EVI curve shown in Fig. 2a represents the seasonality of vegetation growth across the cropland belt from 2001 to 2013 in NSW. The profile and magnitude of the curve and EVI variations are important indicators of vegetation growth. From the average EVI seasonality shown in Fig. 2a, it is apparent that there is only one major growing season across the study area from leaf emergence (start of season; SOS date) at Day of the Year (DoY) 156, which has an EVI value of 0.206, to harvest (end of season; EOS date) at DoY326, which has an EVI value of 0.177. The length of the growing season (LOS) was 170 days, with a maximum EVI value (peak of season; POS) of 0.373 at DoY 246. This indicates that the lengths of vegetative growth (VG) and reproductive growth (RG) were 90 and 80 days, respectively. The actual growing season of winter wheat planted in eastern Australia (Bowden et al., 2008) matches this EVI curve well. At the same time, Fig. 2d shows that the 13 years average EVI profile in thermal time reference, winter crop across the study area appear at 3000 °C degree days and end of senescence at 5500 °C. All the single-year EVI growing season start and end within 500° days with our average fixed growing season. The only differences are the shape and amplitude of the curves.

As Fig. 2b shows, the variation of EVI in the growing season was significantly larger than in the non-growing season, especially during the reproductive growth period, with a Sd of 16.7% at DoY 153 near EOS, 18.2% at DoY 249 near POS, and 19.3% at DoY 257, and the Sd was greater than 20% for the consecutive 8-day time segments from DoY 265 to DoY 313.

3.1.2. The key 8-day time segment of the crop growth cycle

To decide which 8-day segment of EVI in the crop growing season had the strongest correlation with annual yield, we used the Pearson correlation method to analyze the 8-day EVIs and observed wheat grain yield (t ha^{-1}) in NSW at the 117 ground trial sites from 2005 to 2013 for which observational data were available. The 8-day EVIs were positively correlated with the wheat yield throughout the growing season, particularly during the reproductive growth stage (Fig. 2c). The correlation coefficient at the 8-day time segment, start from DoY 153, immediately before leaf emergence was 0.16, and it increased to 0.47 after the heading date (POS) at DoY 249. It increased significantly during the rest of RG and reached its peak at DoY 289, with a value of 0.76. This indicates that the larger the EVI value at DoY 289, the higher the annual yield, and *vice versa*.

The slope of EVI at each 8-day time segment from 2001 to 2013 fluctuated notably during the growing season (Fig. 2c). The slopes were positive during the vegetative growth (VG) phase, but negative during the reproductive phase (RG). Thus, vegetation greenness increased during VG, but decreased during RG. During RG, the trend value dropped by 0.001 each year following POS and then dropped greatest by 0.003 each year at the 8-day time segment, from DoY 257.

As EVI at DoY257 also has a high correlation of 0.56 with annual yield, we identified the two critical 8-day time segments, beginning from DoY257 and DoY 289, as the key 8-day 'windows' during the remotely sensed crop growth cycle.

3.2. Climate and LST seasonality and variability across the NSW wheat-belt in growing season

3.2.1. Climate and LST seasonality and variability

The overall annual climate and LST seasonality patterns (Table 1, Fig. 3) across the NSW wheat belt showed the typical characteristics of a temperate sub-humid climatic zone: warm in the crop pre-growing season (pre-GS) and reproductive phase (RG) and cool in the crop vegetative phase (VG), with moderate rainfall throughout the year. The

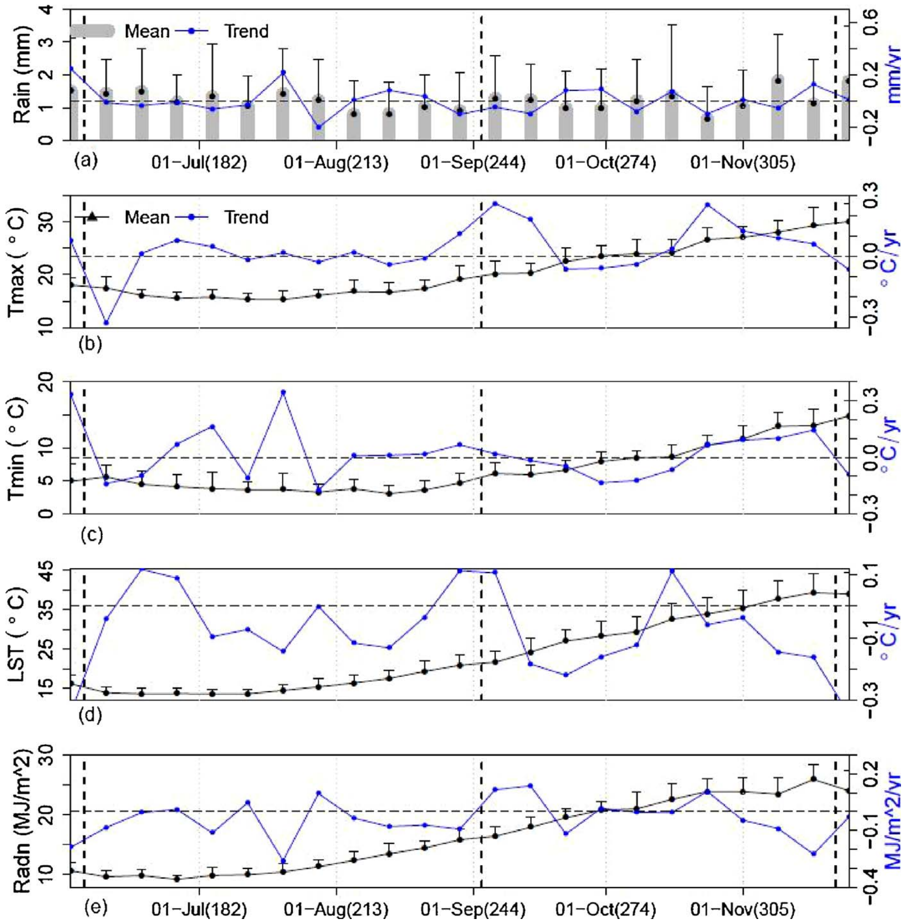

Fig. 3. Growing season climate and LST seasonality as well as their variability and trend at each 8-day time segment from 2001 to 2013 across the NSW cropland belt. (a) Rainfall; (b) maximum air temperature; (c) minimum air temperature; (d) land surface temperature; (e) solar radiation. Black solid curves: seasonality (primary y-axis). Error bars: one standard deviation (Sd). Blue solid curves: trends at each 8-day time segment over 13 years (second y-axis). Black horizontal dash line: 0 line (second y-axis). X-axis: Date (Day of Year). (For interpretation of the references to color in this figure legend, the reader is referred to the web version of this article.)

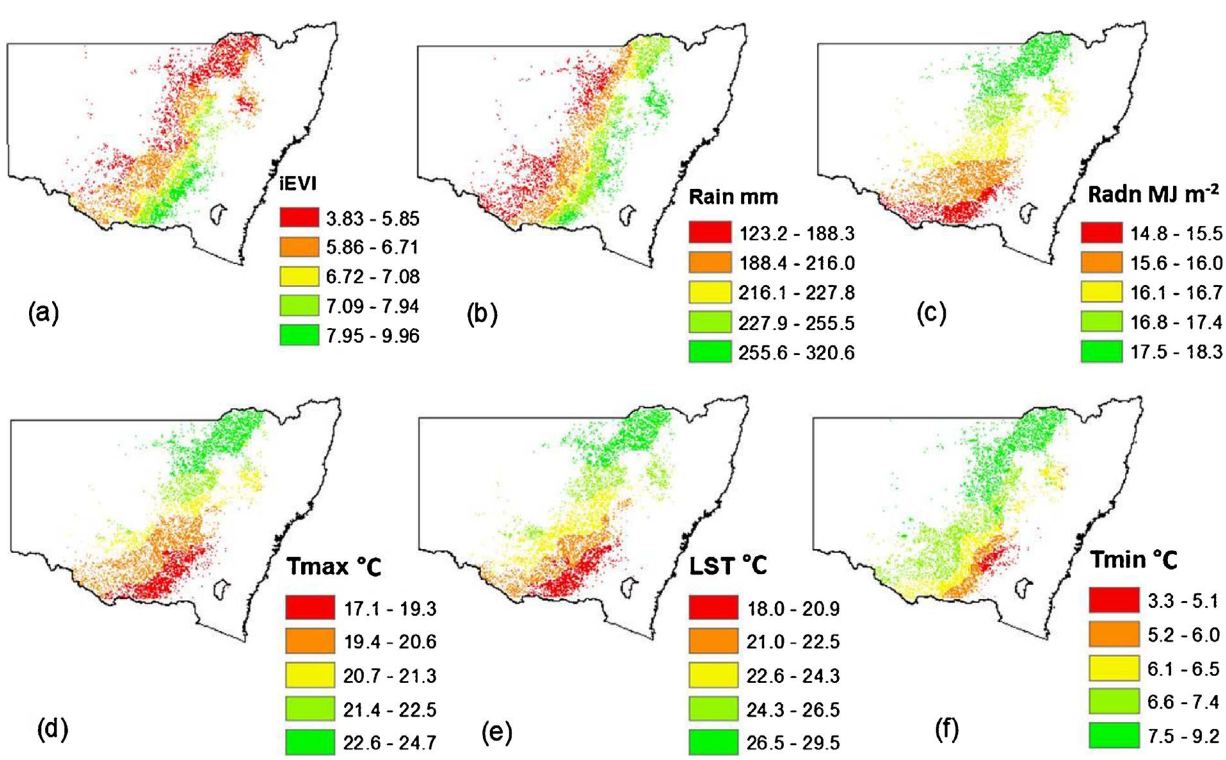

Fig. 4. Spatial variations of the 13-year average iEVI as well as growing season climate and LST conditions. (a) iEVI; (b) rainfall; (c) radiation; (d) maximum air temperature; (e) land surface temperature; (f) minimum air temperature.

average rainfall (Rain) during the VG and RG was 114.1 and 99.5 mm, respectively, across the study area, and in pre-GS, the average was 182.4, with a moderately even distribution throughout the crop growing season. The ranges of the average daily T_{max}, T_{min}, Radn, and LST (canopy temperature) throughout the GS were 30.1–15.3 °C, 14.8–3.1 °C, 25.9–9.2 MJ m^{-2}, and 39.4–13.7 °C, respectively. The Sd values of T_{max}, LST and Radn in RG were mostly higher than those during the VG phase (Fig. 3), while the variability of T_{min} was larger at the beginning and end of the GS relative to the middle stages of the GS. The variability of rain was irregular throughout the GS and peaked at the 8-day time segment from DoY 289, with a Sd of 159%. The Sd provided in Table 1 shows the overall climate and LST variability at a broader time-scale. All of the Sds in the RG phase were much larger than those of the pre-GS and VG phases (Table 1). The variability of the climate and LST in the VG was the lowest. LST showed the largest variability among all climate components, especially during the RG (Table 1).

During the 32nd 8-day period, near the heading date (DoY249), all of the heat factors, T_{max}, T_{min}, LST and Radn, showed an increasing trend from 2001 to 2013 (Fig. 3), with slopes of 0.26 °C y^{-1}, 0.02 °C y^{-1}, 0.11 °C y^{-1} and 0.12 MJ m^{-2} y^{-1}, respectively. The EVI started to decrease at this time point (Fig. 2), with a decreasing rate of 0.001 y^{-1}. At the critical 8-day time segment from DoY 257, T_{min} and LST showed decreasing trends, with annual rates of 0.02 °C y^{-1} and 0.18 °C y^{-1}. Meanwhile, Radn and T_{max} showed increasing trends, with annual rates of 0.14 MJ/m^2/yr and 0.18 °C y^{-1}, respectively. At the other critical 8-day time segment from DoY 289, T_{max} and T_{min} had the same trends as at the 8-day segment from DoY 257. However, LST had an increasing trend, with a rate of 0.11 °C y^{-1}, and Radn had a decreasing trend, with a rate of 0.01 MJ m^{-2} y^{-1}.

3.2.2. Spatial variation of the 13-year average iEVI and climate conditions

The average annual iEVI across the NSW cropland belt ranged from 3.84 to 9.96 (Fig. 4). The iEVI in the southeastern part of the study area was almost twice as large compared with the upper northern part, with an average value of 8.9 in the southeast and 4.8 in the upper north part of the NSW wheat belt.

Correspondence was observed for the spatial distribution of rainfall in the southern part, but not in the northern part, of study area. The average annual rainfall during the GS ranged from 123.2 mm in the west to 320.6 mm in the east and displayed a typical E-W spatial gradient that was distributed based on the pixels' distance to the coast. The growing season Radn, T_{max}, LST and T_{min} followed a similar N-S temperature spatial gradient distribution pattern, which was higher in the north and lower in the southeast. Their range differences were 3.5 MJ m^{-2}, 7.6 °C, 11.5 °C, 5.9 °C, respectively.

3.3. Contributions of climate and LST variability to crop growth variation over the GS

3.3.1. Individual impacts of climate and LST on EVI variation at a regional scale

Fig. 5 shows the partial correlations at an 8-day time-scale during the growing season across the entire study area. The correlation was statistically significant when its r value was greater than +0.553 or lower than −0.553 (Plant, 2012).

Generally, inter-annual variability of EVI was positively correlated with Rain, T_{min}, and Radn and negatively correlated with T_{max} and LST. The correlation of the inter-annual variability and Sa-s between rain and EVI steadily increased throughout the crop growing season. The correlation of T_{max}-EVI and T_{min}-EVI in the crop growing season showed inverse patterns. The amplitude of the absolute values of the T_{max}-EVI correlation coefficients was larger than those of T_{min}-EVI. The correlation coefficients of the 8-day LST-EVI in the vegetative growth phase (VG) were more moderate and smaller in terms of absolute values than those during the reproductive growth phase (RG) and reached −0.97 at the 8-day time segment from DoY 289. The highest point of the Radn-EVI correlation coefficient was also at that segment, with a value of 0.78.

As shown in Fig. 5, more significant and marginally significant correlations between the 8-day EVI Sa-s and climate and LST Sa-s were observed during the RG than during the VG. At the critical 8-day time segment from DoY 257, in Section 3.1.2 we identified that rain was significantly and positively correlated with EVI, while it was significantly and negatively correlated with LST. At another critical 8-day segment from DoY 289, LST-EVI and Radn-EVI showed significant divergent correlations. The T_{max}-EVI correlations were significant and negative twice during the VG and 3 times during the RG.

3.3.2. Accumulated relative contributions of the climate variability to the EVI variability

Fig. 6 shows the contributions of the inter-annual climate variation to variations in EVI at the 8-day time scale during the growing season (GS). The total effects of climate variation showed an increasing trend throughout the GS and accounted for 83.3% at the 8-day time segment from DoY 169 during the VG and 97.1% at the segment from DoY 289 during the RG on EVI Sa-s across the NSW croplands belt. At the critical time segment from DoY 257, the total climatic contribution increased from 47.6% from the previous 8-day time segment to 88.3%, while the EVI value dropped sharply by 0.003 each year (Fig. 2c).

In the rainfed NSW cropland belt, the proportion of rain Sa-s to the total climate contributions peaked at the 8-day time segment from DoY 169, which was the tillering stage of the vegetative growth phase (VG), with a value of 50.6%, and then declined steadily throughout the VG and increased moderately during the reproductive growth phase (RG). At the critical 8-day window from DoY 257, it accounted for 21.8% of the variation in the EVI. The proportion of the LST variation among the total climate contribution increased from the VG to the RG and accounted for 65.8% at the critical 8-day window from DoY 289. It was more than half of the total climate contribution at that time segment. During the RG, the LST was the single most important climate factor that affected EVI variability in 9 out of 10 8-day time segments across the NSW cropland belt.

T_{min} explained a large proportion of the impact of climate variation on the change in EVI immediately before peak of the season date (POS), the corresponding crop heading date. It reached its peak at the 8-day time segment from DoY 233, with a value of 46.5%. The contribution of T_{max} variation to the EVI Sa-s was larger during the RG than the VG, but more moderate than the LST Sa-s. It peaked at the 8-day time segment from DoY 265, with a value of 37.3%. Radn Sa-s affected the EVI Sa-s steadily from approximately 10% to 20% throughout the GS across the study area.

3.3.3. Spatial distribution of the climate and LST variability contributions to EVI variation

The individual and accumulated contributions of climate and LST Sa-s to EVI Sa-s at every selected pixel during the GS were demonstrated in Fig. 7. The inter-annual total climate variability at the 8-day time scale caused EVI variations from 5.94% to 42.09% across the study area from 2001 to 2013. The total effects were higher in the north and southwestern parts of the NSW wheat belt relative to the middle parts.

Variation in LST was the most important climate factor influencing variation in EVI. The contribution ranged from 3.24% to 34.47% across the cropland belt in NSW. The spatial distribution was largest in the northern and southwestern parts of the study area. The relative importance of the total variability of total rain was smaller, with a maximum contribution of 3.57% to EVI variation, and its importance was larger in the western and middle parts of the NSW wheat belt. The importance of variation in Radn that caused variability in EVI was largest on the eastern parts of the cropland belt, with a range from 0.2% to 3.27%. The contribution range of T_{max} was 0.28% to 10.27%, with a gradual trend from east to west. The effects of T_{min} Sa-s ranged from

Agriculture, Ecosystems and Environment 254 (2018) 99–110

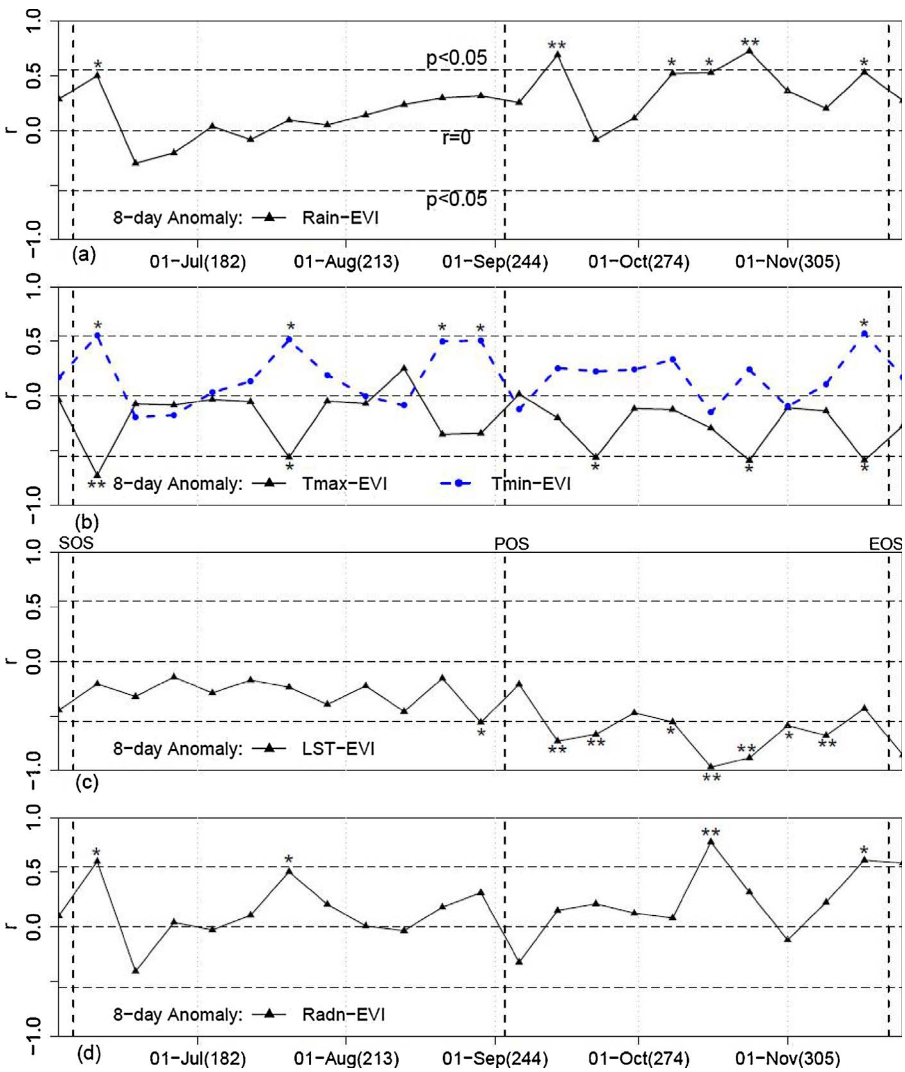

Fig. 5. Partial correlations between standardized anomalies (Sa-s) of 8-day EVI and individual climate components in the growing seasons from 2001 to 2013. (a) rainfall; (b) maximum air temperature and minimum air temperature; (c) land surface temperature; (d) radiation. Horizontal dash lines: significance threshold where p = 0.05. *: p < 0.1, marginal significant. **: p < 0.05, significant. X-axis: Date (Day of the Year).

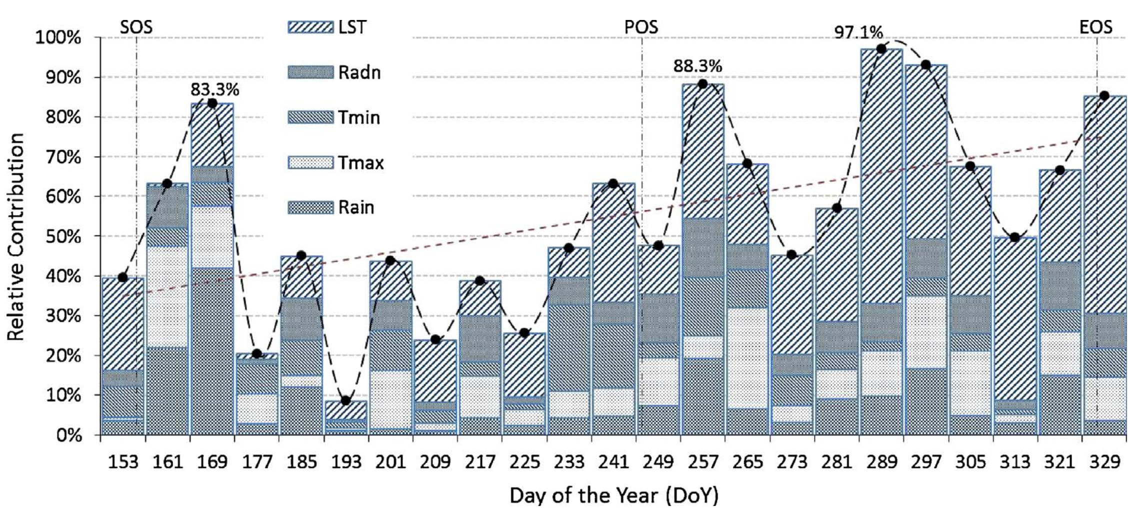

Fig. 6. Individual and accumulated contributions of the climate and LST variability to the variation of EVI at the 8-day time scale in the growing season over 13 years. Stacked bars: individual contributions; black curve: accumulated contribution; brown dashed line: trend of accumulated contribution. (For interpretation of the references to color in this figure legend, the reader is referred to the web version of this article.)

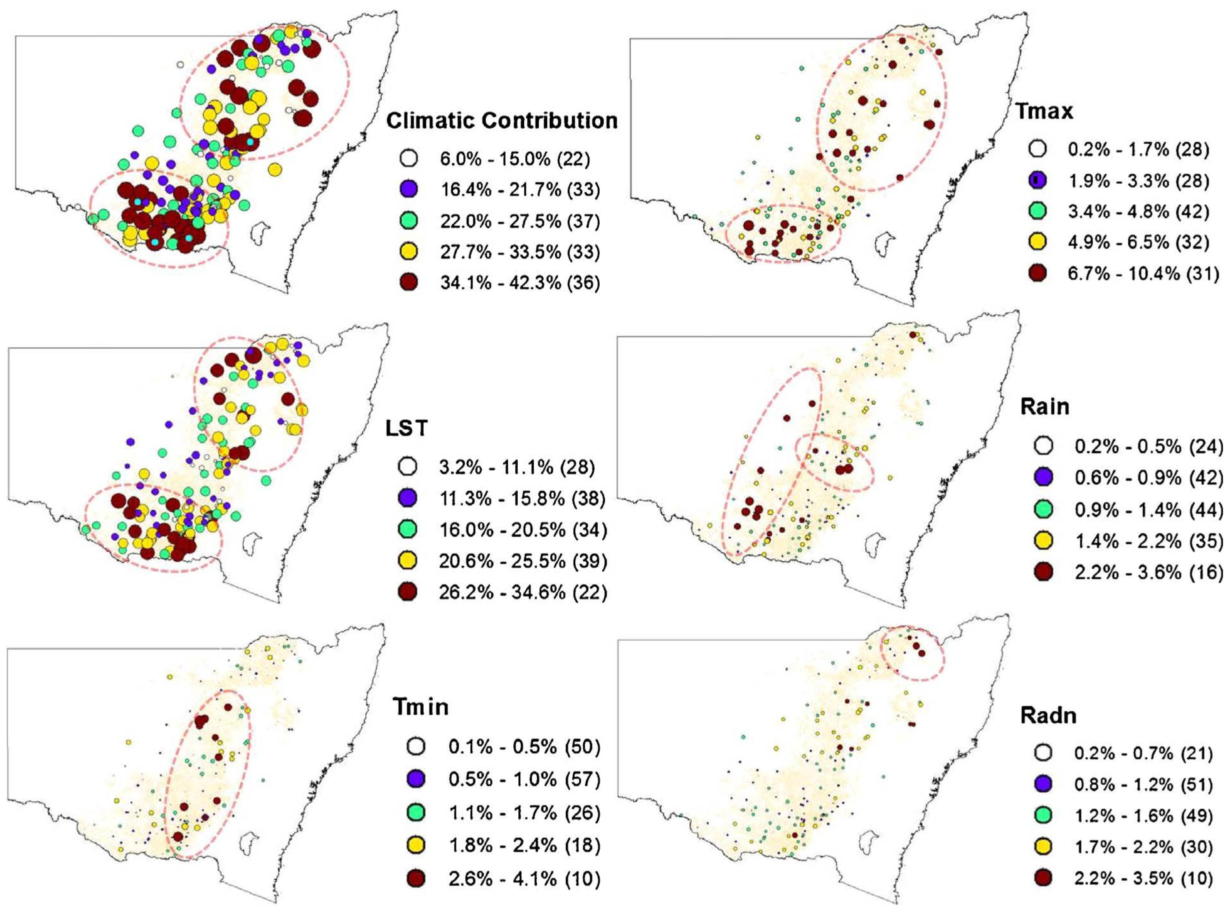

Fig. 7. Spatial distributions of the contributions of climate and LST standard anomalies (Sa-s) to EVI Sa-s in the growing season across the NSW cropland belts. Number in brackets: counts of tested pixels for which their attributes were in the corresponding range, and 161 pixels in total were tested.

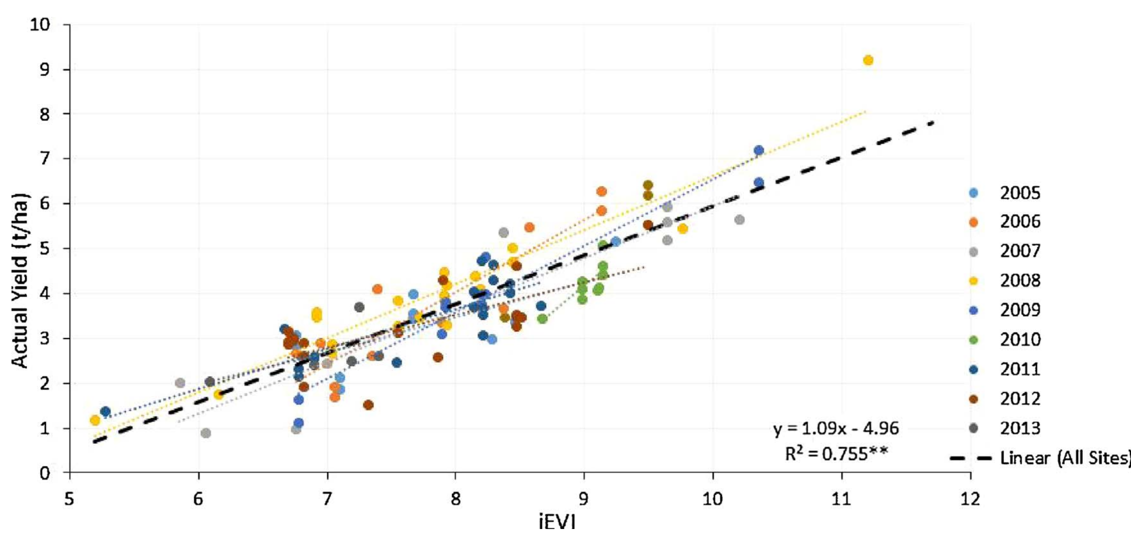

Fig. 8. Scatterplots between the actual yield and iEVI for 117 trial sites and their linear regression lines. **: p value < 0.001.

0.08% to 4.08% for EVI Sa-s across the study area, and they were greater in the relatively cooler areas of the southeastern and middle parts of the study area.

4. Discussion

4.1. Ability of the MODIS EVI profile to represent rainfed cropland productivity in Australia

The start and end dates of the growth season (SOS and EOS) of winter crops are relatively fixed compared to the considerable variability observed in native grasses and shrubs (Bowden et al., 2008). SOS and EOS are not merely determined by climate because human management and farmers' experience can largely control them. Although there is sowing date guidance offered based on rainfall (Keating et al., 2002), farmers still sow even if rainfall does not reach the required levels during June to avoid heat stress in the following summer. Variations in the timing of the different growth stages are thereafter largely affected by climate variability, especially in broadacre rainfed cropping systems. The EVI profile in thermal time reference has shown the relatively fixed growing season across the NSW wheat belt, we could measure the relative contributions of climate variation to crop growth variability at every 8-day time segment.

The MODIS EVI-fitted GS in this study starts at DoY 156 in early June ends at DoY 326 in late November, with a length of 170 days. The average peak of season (POS) date occurs at DoY 246 in September, with an EVI value of 0.373. This phenology matches well with the observed wheat life cycle in eastern Australia (Bowden et al., 2008). Based on observations of 117 trials, the average sowing and harvest dates across the NSW wheat belt are DoY 145 (± 1.5 days) and DoY 326 (± 1.2 days), respectively. There could be an allowance of 11 days for seeds to establish from the sowing date to the leaf emergence date (SOS, DoY156). The average harvest date had the same date with the MODIS EVI derived end of season (EOS) date, DoY 326. Meanwhile, the iEVI was significantly and linearly correlated with the *in-situ* grain yield among the trials each year as well as among all sites (Fig. 8). The overall R^2 was 0.755, while the relationship best fit the 11 trials in year 2009, with an R^2 of 0.940. These results not only indicate that wheat is the largest major winter crop planted across the NSW cropland but also indicate that the MODIS EVI is capable of monitoring the winter wheat growth cycle in broadacre rainfed cropping systems.

The ability of the MODIS EVI to capture information related to crop growth and development has also been tested (Bolton and Friedl, 2013) in the central United States. The authors concluded that MODIS products have good potential applications for agricultural monitoring in areas with large field sizes, as is the case in Australian wheat cropping in NSW. The MODIS-derived average annual time-series profile of the EVI (Fig. 2a) reflects the actual crop growth conditions across the NSW wheat belt. Over the entire crop life span, the correlation coefficient between EVIs and the actual yield peaks at the 8-day time segment from DoY 289, with a value of 0.76 (Fig. 2c). Thus, the stability and range of EVI values at this critical time segment had the highest direct correlation and ensured an annual attainable yield.

4.2. Impacts of climate and LST variability on the variation of the EVI in key crop growth stages

The trend of EVI values at every 8-day segment can be explained not only by the delayed/advance of the growing season but also by the technological improvement that modifies wheat crop traits as well as the interference of weather extremes on crop radiometric reflection. From 2001 to 2013, farmers improved the biomass of wheat crops during vegetative growth phase (VG) across the NSW cropland belt, but neglected the importance of plant biomass accumulation during the reproductive growth phase (RG) (Fig. 2c). The sharpest drop of EVI at the 8-day time segment from DoY 257 made it the most sensitive to climate variability during this period.

The relative importance of the proportion of rain, T_{max}, T_{min}, Radn and LST Sa-s to EVI Sa-s reached its peak at the 8-day time segments from DoY 169 (VG), DoY 265 (RG), DoY 233 (VG), DoY 217 (VG), and DoY 289 (RG), respectively (Fig. 6), across the NSW wheat belt during 2001–2013. In the semi-arid rain-fed environment, the lack of rainfall and resultant water stress is inevitably one of the most serious climatic limiting factors to crop establishment and development (Asseng et al., 2011), especially around the tilling stage (the 8-day time segment from DoY 169, where Rain is the most important climate factor) during VG. However, during RG, heat stress is more evident because temperature has a relatively higher base during this phase, which is sometimes higher than the optimum wheat growth air temperature of 23 °C (www.agric.wa.gov.au). The cropland maximum air temperature and canopy temperature reached > 30 °C during the RG (Fig. 3) across the study area. In particular, fluctuations of T_{max} and LST during a sensitive stage of crop development, such as the grain growth stage (the 8-day time segment from DoY289), can significantly reduce grain yield due to their direct effects on leaf photosynthesis, grain number and grain mass (Talukder et al., 2014), while a continuous period of extremely high temperatures can result in physiological damage and almost total yield loss (Asseng et al., 2011; Lobell et al., 2012). At the critical 8-day segments from DoY 257 and 289, identified in this study (part 3.1.2), which corresponded to the wheat flowering and grain growth stages, respectively, the impacts of heat variation outweighed the impact of variation in rainfall on EVI by more than twofold.

During RG, variation of LST was the most important factor that contributed to variation of EVI. LST, the canopy temperature, quantifies the combined indirect effects of air temperature, radiation and effective rainfall within the soil-plant-atmosphere continuum. A higher LST reflects lower latent heat flux from the canopy, which indicates lower canopy evapotranspiration and higher heat stress conditions (Li et al., 2010). The remotely sensed estimation of surface temperature has proven to be a well suited ground canopy temperature indicator in large-scale crop monitoring (Karnieli et al., 2010; Sandholt et al., 2002). It simultaneously measures the comprehensive water and heat stress conditions caused by interactions among climatic driving factors. Thus, the impacts of the LST variation on the variation of the EVI increased in the hotter northern and drier southwestern parts of the NSW wheat belt.

5. Conclusions

In this study, we quantified the spatio-temporal impacts of variation in climate and land surface temperature (LST) on the variation of crop EVI at key crop growth stages. The standard anomaly method was adopted to indicate the variability of all variables at an 8-day time scale. We found that a single major crop growing season (GS), occurred in the second half of the year across the NSW wheat belt during 2001–2013. Two critical 8-day time segments, beginning from DoY 257 and 289, were identified as the key 'windows' during the winter crop GS, that is, the variation in climate during these 8-day time segments exerted a greater impact on the grain yield than during any other periods during the GS.

Our results show that the total climate variation during the two 8-day 'windows' contributed more than 88% of the variability in EVI, of which the LST accounted for more than half. Therefore, more attention should be paid to the LST during implementation of large-scale rainfed cropland monitoring. As such, once an association model (*i.e.* linear regression model) among LST, EVI and annual grain yield is built-up (Kumar, 1998), we could estimate and predict grain yield during these two key 8-day "windows" (approximately one month) before the crop is harvested. Spatially, the total contribution of climate variation during the GS accounted for up to 42% of the variability in the EVI, especially in the northern and southwestern regions of the NSW wheat belt. As an index that integrates the indirect effects of the complex interactions among all the climate-driving factors on crop growth, the LST is the first dominant climate component that affects the variability of the EVI across those regions.

The limitation of this study was the limited years (13 years) of data, which could cause over-fitted models in the analysis. Because the time period from 2001 to 2013 was the period that saw a shift from extreme drought to flood at a surprising speed (Dijk et al., 2013), the shift was typically significant. We thereafter targeted this specific period of time and evaluated the relationship between climate and crop growth in variability. This study also narrowed the analyze time slot from annual to 8-days, which is the attainable temporal scale by MODIS EVI and LST, to make it possible investigating the diverse crop-climate relationship over the crop life span. However, in consideration of the comparison of the model performance among this time period (2001–2013) and other years before and after, we will adopt additional datasets to expand the number of sample years and build the best fit model in the future.

Acknowledgements

The Authors wish to thank Dr. Hao Shi, Dr. Zunyi Xie and Dr. Mingming Cheng for their helpful suggestions with this study. We are grateful to Grains Research and Development Corporation (GRDC) National Variety Trials (NVT), Australia (http://www.nvtonline.com.au/) for their data support. The first author acknowledges the financial support from Chinese Scholarship Council, Ministry of Education, China, as well as Dr. Sabina Belli and Mrs Ann-Maree Dombroski for their suggestions on the grammar of this paper.

References

Australian Bureau of Agriculture and Resources Economics and Science (ABARES), 2017. http://www.agriculture.gov.au.abares, Last accessed: Jan 2017.
Anwar, M.R., O'Leary, G., McNeil, D., Hossain, H., Nelson, R., 2007. Climate change impact on rainfed wheat in south-eastern Australia. Field Crops Res. 104 (1–3), 139–147.
Asseng, S., Foster, I.A.N., Turner, N.C., 2011. The impact of temperature variability on wheat yields. Glob. Change Biol. 17 (2), 997–1012.
Atwell, B.J., 1999. Plants in Action: Adaptation in Nature, Performance in Cultivation. Macmillan Education, AU.
Barlow, K.M., Christy, B.P., O'Leary, G.J., Riffkin, P.A., Nuttall, J.G., 2015. Simulating the impact of extreme heat and frost events on wheat crop production: a review. Field Crops Res. 171, 109–119.
Biradar, C.M., Thenkabail, P.S., Noojipady, P., Li, Y., Dheeravath, V., Turral, H., Velpuri, M., Gumma, M.K., Gangalakunta, O.R.P., Cai, X.L., Xiao, X., Schull, M.A., Alankara, R.D., Gunasinghe, S., Mohideen, S., 2009. A global map of rainfed cropland areas (GMRCA) at the end of last millennium using remote sensing. Int. J. Appl. Earth Obs. Geoinf. 11 (2), 114–129.
Bolton, D.K., Friedl, M.A., 2013. Forecasting crop yield using remotely sensed vegetation indices and crop phenology metrics. Agric. For. Meteorol. 173, 74–84.
Bowden, P., Edwards, J., Ferguson, N., Nee, T.M., Manning, B., Roberts, K., Schipp, A., Schulze, K., Wilkins, J., 2008. Wheat Growth and Development. NSW Department of Primary Industries.
Broich, M., Huete, A., Paget, M., Ma, X., Tulbure, M., Coupe, N.R., Evans, B., Beringer, J., Devadas, R., Davies, K., 2015. A spatially explicit land surface phenology data product for science, monitoring and natural resources management applications. Environ. Model. Softw. 64, 191–204.
Calzadilla, A., Rehdanz, K., Betts, R., Falloon, P., Wiltshire, A., Tol, R.J., 2013. Climate change impacts on global agriculture. Clim. Change 120 (1–2), 357–374.
Chevan, A., Sutherland, M., 1991. Hierarchical partitioning. Am. Stat. 45 (2), 90–96.
Cleverly, J., Eamus, D., Luo, Q., Restrepo Coupe, N., Kljun, N., Ma, X., Ewenz, C., Li, L., Yu, Q., Huete, A., 2016. The importance of interacting climate modes on Australia's contribution to global carbon cycle extremes. Sci. Rep. 6, 23113.
Cohn, A.S., VanWey, L.K., Spera, S.A., Mustard, J.F., 2016. Cropping frequency and area response to climate variability can exceed yield response. Nat. Clim. Change 6 (6), 601–604.
Cong, N., Wang, T., Nan, H., Ma, Y., Wang, X., Myneni, R.B., Piao, S., 2013. Changes in satellite-derived spring vegetation green-up date and its linkage to climate in China from 1982 to 2010: a multimethod analysis. Glob. Change Biol. 19 (3), 881–891.
Dijk, A.I., Beck, H.E., Crosbie, R.S., Jeu, R.A., Liu, Y.Y., Podger, G.M., Timbal, B., Viney, N.R., 2013. The Millennium Drought in southeast Australia (2001-2009): natural and human causes and implications for water resources, ecosystems, economy, and society. Water Resour. Res. 49 (2), 1040–1057.
Duveiller, G., Baret, F., Defourny, P., 2013a. Using thermal time and pixel purity for enhancing biophysical variable time series: an interproduct comparison. IEEE Trans. Geosci. Remote Sens. 51 (4), 2119–2127.
Duveiller, G., López-Lozano, R., Baruth, B., 2013b. Enhanced processing of 1-km spatial resolution fAPAR time series for sugarcane yield forecasting and monitoring. Remote Sens. 5 (3), 1091.
Eamus, D., Huete, A., Yu, Q., 2016. Vegetation Dynamics: A Synthesis of Plant Ecophysiology Remote Sensing and Modelling. Cambridge University Press, pp. 43–341.
Field, C.B., Barros, V.R., Mach, K., Mastrandrea, M., 2014. Climate change 2014: impacts, adaptation, and vulnerability. Contribution of Working Group II to the Fifth Assessment Report of the Intergovernmental Panel on Climate Change.
Franch, B., Vermote, E.F., Becker-Reshef, I., Claverie, M., Huang, J., Zhang, J., Justice, C., Sobrino, J.A., 2015. Improving the timeliness of winter wheat production forecast in the United States of America, Ukraine and China using MODIS data and NCAR Growing Degree Day information. Remote Sens. Environ. 161 (Suppl. C), 131–148.
Godfray, H.C.J., Beddington, J.R., Crute, I.R., Haddad, L., Lawrence, D., Muir, J.F., Pretty, J., Robinson, S., Thomas, S.M., Toulmin, C., 2010. Food security: the challenge of feeding 9 billion people. Science 327 (5967), 812–818.
Gong, Z., Kawamura, K., Ishikawa, N., Goto, M., Wulan, T., Alateng, D., Yin, T., Ito, Y., 2015. MODIS normalized difference vegetation index (NDVI) and vegetation phenology dynamics in the Inner Mongolia grassland. Solid Earth 6, 1185–1194.
Grömping, U., 2006. Relative importance for linear regression in R: the package relaimpo. J. Stat. Softw. 17 (1), 1–27.
Guo, L., An, N., Wang, K., 2016. Reconciling the discrepancy in ground- and satellite-observed trends in the spring phenology of winter wheat in China from 1993 to 2008. J. Geophys. Res.: Atmos. 121 (3), 1027–1042.
Hamblin, A., 2009. Policy directions for agricultural land use in Australia and other post-industrial economies. Land Use Policy 26 (4), 1195–1204.
Huete, A.R., 2012. Vegetation indices, remote sensing and forest monitoring. Geogr. Compass. 6 (9), 513–532.
Huete, A., Didan, K., Miura, T., Rodriguez, E.P., Gao, X., Ferreira, L.G., 2002. Overview of the radiometric and biophysical performance of the MODIS vegetation indices. Remote Sens. Environ. 83 (1-2), 195–213.
Hochman, Z., Gobbett, D.L., Horan, H., 2017. Climate trends account for stalled wheat yields in Australia since 1990. Glob. Change Biol. 23, 2071–2081.
Karnieli, A., Agam, N., Pinker, R.T., Anderson, M., Imhoff, M.L., Gutman, G.G., Panov, N., Goldberg, A., 2010. Use of NDVI and land surface temperature for drought assessment: merits and limitations. J. Clim. 23 (3), 618–633.
Keating, B.A., Gaydon, D., Huth, N.I., Probert, M.E., Verburg, K., Smith, C.J., Bond, W., 2002. Use of modelling to explore the water balance of dryland farming systems in the Murray-Darling Basin, Australia. Eur. J. Agron. 18 (1–2), 159–169.
Kumar, V., 1998. An early warning system for agricultural drought in an arid region using limited data. J. Arid Environ. 40 (2), 199–209.
Lawrence, G., Richards, C., Lyons, K., 2013. Food security in Australia in an era of neoliberalism, productivism and climate change. J. Rural Stud. 29, 30–39.
Li, L., Nielsen, D.C., Yu, Q., Ma, L., Ahuja, L.R., 2010. Evaluating the Crop Water Stress Index and its correlation with latent heat and CO2 fluxes over winter wheat and maize in the North China plain. Agric. Water Manag. 97 (8), 1146–1155.
Li, Z.-L., Tang, B.-H., Wu, H., Ren, H., Yan, G., Wan, Z., Trigo, I.F., Sobrino, J.A., 2013. Satellite-derived land surface temperature: current status and perspectives. Remote Sens. Environ. 131, 14–37.
Lobell, D.B., Sibley, A., Ivan Ortiz-Monasterio, J., 2012. Extreme heat effects on wheat senescence in India. Nat. Clim. Change 2 (3), 186–189.
Lymburner, L., Tan, P., Mueller, N., Thackway, R., Lewis, A., Thankappan, M., Randall, L., Islam, A., Senarath, U., 2010. 250 Metre Dynamic Land Cover Dataset of Australia. Geoscience Australia, Canberra.
Ma, Y., Wang, S., Zhang, L., Hou, Y., Zhuang, L., He, Y., Wang, F., 2008. Monitoring winter wheat growth in North China by combining a crop model and remote sensing data. Int. J. Appl. Earth Obs. Geoinf. 10 (4), 426–437.
Ma, X., Huete, A., Yu, Q., Coupe, N.R., Davies, K., Broich, M., Ratana, P., Beringer, J., Hutley, L.B., Cleverly, J., 2013. Spatial patterns and temporal dynamics in savanna vegetation phenology across the North Australian Tropical Transect. Remote Sens. Environ. 139, 97–115.
Ma, X., Huete, A., Moran, S., Ponce-Campos, G., Eamus, D., 2015. Abrupt shifts in phenology and vegetation productivity under climate extremes. J. Geophys. Res.: Biogeosci. 2036–2052.
Ma, X., Huete, A., Cleverly, J., Eamus, D., Chevallier, F., Joiner, J., Poulter, B., Zhang, Y., Guanter, L., Meyer, W., Xie, Z., Ponce-Campos, G., 2016. Drought rapidly diminishes the large net CO(2) uptake in 2011 over semi-arid Australia. Sci. Rep. 6, 37747.
Moulin, S., Bondeau, A., Delecolle, R., 1998. Combining agricultural crop models and satellite observations: from field to regional scales. Int. J. Remote Sens. 19 (6), 1021–1036.
Piao, S., Fang, J., Zhou, L., Philippe, C., Zhu, B., 2006. Variations in satellite-derived phenology in China's temperate vegetation. Glob. Change Biol. 12 (4), 672–685.
Plant, R.E., 2012. Spatial Data Analysis in Ecology and Agriculture Using R. CRC Press, Boca Raton, Florida.
Ponce Campos, G.E., Moran, M.S., Huete, A., Zhang, Y., Bresloff, C., Huxman, T.E., Eamus, D., Bosch, D.D., Buda, A.R., Gunter, S.A., Scalley, T.H., Kitchen, S.G., McClaran, M.P., McNab, W.H., Montoya, D.S., Morgan, J.A., Peters, D.P.C., Sadler, E.J., Seyfried, M.S., Starks, P.J., 2013. Ecosystem resilience despite large-scale altered hydroclimatic conditions. Nature 494 (7437), 349–352.
Potgieter, A., Apan, A., Hammer, G., Dunn, P., 2011. Estimating winter crop area across seasons and regions using time-sequential MODIS imagery. Int. J. Remote Sens. 32 (15), 4281–4310.
Rabbinge, R., 2007. The ecological background of food production. In: Ciba Foundation Symposium 177 – Crop Protection and Sustainable Agriculture. John Wiley & Sons, Ltd.. pp. 2–29.
Ray, D.K., Gerber, J.S., MacDonald, G.K., West, P.C., 2015. Climate variation explains a third of global crop yield variability. Nat. Commun. 6.
Reed, B.C., Brown, J.F., VanderZee, D., Loveland, T.R., Merchant, J.W., Ohlen, D.O., 1994. Measuring phenological variability from satellite imagery. J. Veg. Sci. 5 (5), 703–714.
Rosenzweig, C., Jones, J., Hatfield, J., Ruane, A., Boote, K., Thorburn, P., Antle, J., Nelson, G., Porter, C., Janssen, S., 2013. The agricultural model intercomparison and improvement project (AgMIP): protocols and pilot studies. Agric. For. Meteorol. 170, 166–182.
Sakamoto, T., Yokozawa, M., Toritani, H., Shibayama, M., Ishitsuka, N., Ohno, H., 2005. A crop phenology detection method using time-series MODIS data. Remote Sens. Environ. 96 (3–4), 366–374.
Sakamoto, T., Gitelson, A.A., Arkebauer, T.J., 2013. MODIS-based corn grain yield estimation model incorporating crop phenology information. Remote Sens. Environ. 131, 215–231.
Sandholt, I., Rasmussen, K., Andersen, J., 2002. A simple interpretation of the surface temperature/vegetation index space for assessment of surface moisture status. Remote Sens. Environ. 79 (2–3), 213–224.

Shumway, R.H., Stoffer, D.S., 2010. Time Series Analysis and Its Applications: With R Examples. Springer Science & Business Media.
Skakun, S., Franch, B., Vermote, E., Roger, J.-C., Becker-Reshef, I., Justice, C., Kussul, N., 2017. Early season large-area winter crop mapping using MODIS NDVI data, growing degree days information and a Gaussian mixture model. Remote Sens. Environ. 195 (Suppl. C), 244–258.
Stokes, C., Howden, M., 2010. Adapting Agriculture to Climate Change: Preparing Australian Agriculture, Forestry and Fisheries for the Future. CSIRO Publishing.
Suepa, T., 2013. Satellite time-series data for vegetation phenology detection and environmental assessment in Southeast Asia. Michigan State University PhD thesis.
Talukder, A.S.M.H.M., McDonald, G.K., Gill, G.S., 2014. Effect of short-term heat stress prior to flowering and early grain set on the grain yield of wheat. Field Crops Res. 160, 54–63.
Tripathi, A., Tripathi, D.K., Chauhan, D.K., Kumar, N., Singh, G.S., 2016. Paradigms of climate change impacts on some major food sources of the world: a review on current knowledge and future prospects. Agric. Ecosyst. Environ. 216, 356–373.
Wan, Z., Wang, P., Li, X., 2004. Using MODIS Land Surface Temperature and Normalized Difference Vegetation Index products for monitoring drought in the southern Great Plains, USA. Int. J. Remote Sens. 25 (1), 61–72.
Wang, B., Chen, C., Liu, D.L., Asseng, S., Yu, Q., Yang, X., 2015a. Effects of climate trends and variability on wheat yield variability in eastern Australia. Clim. Res. 64 (2), 173.
Wang, B., Liu, D.L., Asseng, S., Macadam, I., Yu, Q., 2015b. Impact of climate change on wheat flowering time in eastern Australia. Agric. For. Meteorol. 209–210, 11–21.
Wardlow, B.D., Egbert, S.L., 2008. Large-area crop mapping using time-series MODIS 250 m NDVI data: an assessment for the U.S. Central Great Plains. Remote Sens. Environ. 112 (3), 1096–1116.
Xie, Z., Huete, A., Restrepo-Coupe, N., Ma, X., Devadas, R., Caprarelli, G., 2016. Spatial partitioning and temporal evolution of Australia's total water storage under extreme hydroclimatic impacts. Remote Sens. Environ. 183, 43–52.
Yu, Q., Hengsdijk, H., Liu, J.D., 2001. Application of a progressive-difference method to identify climatic factors causing variation in the rice yield in the Yangtze Delta, China. Int. J. Biometeorol. 45 (2), 53–58.
Yu, Q., Li, L., Luo, Q., Eamus, D., Xu, S., Chen, C., Wang, E., Liu, J., Nielsen, D.C., 2014. Year patterns of climate impact on wheat yields. Int. J. Climatol. 34 (2), 518–528.
Zheng, B., Chenu, K., Fernanda Dreccer, M., Chapman, S.C., 2012. Breeding for the future: what are the potential impacts of future frost and heat events on sowing and flowering time requirements for Australian bread wheat (Triticum aestivium) varieties? Glob. Change Biol. 18 (9), 2899–2914.